scientific reports

Check for updates

OPEN

High-intensity interval training alleviates STZ-induced muscle atrophy by restoration of nuclear positioning defects in C57BL/6 male mice

Masoud Rahmati[1,2]✉ & Rohollah Nikooie[3]✉

We tested the hypothesis that improper myonuclei arrangement and morphology are involved in diabetes-induced myofiber atrophy and whether and how high-intensity interval training (HIIT) affects these impairments in isolated skeletal muscle myofibers. STZ-induced diabetes decreased muscle fiber cross-sectional area (CSA) mediated by reduced myonuclear number, enhanced nuclear apoptotic, and failed nuclear accretion from satellite cells. STZ-induced muscle atrophy was accompanied by improper nuclear positioning (sinus of the maximum diameter angles and distance between adjacent myonuclei) and morphology (maximum diameter, area, and volume of the nuclei), which was mediated by suppressed expression of proteins involved in nuclear positioning including KIF5B, dynein, and Nesprin1. Disturbing nuclear positioning by inhibition of Kinsein1 activity reduced CSA to a greater extent than in diabetes alone, suggesting STZ-induced muscle atrophy is mediated by changes in nuclear positioning. HIIT alleviated the STZ-induced decline in muscle CSA and myonuclei per fiber by restoring myonuclear morphometry impairments and improper nuclear positioning to the normal level. HIIT-induced increase in muscle CSA deterred by inhibition of Kinesin1 activity, suggesting its effect is mediated by proper nuclear positioning. These findings suggest that normal nuclear positioning are required for the changes in fiber size properties associated with HIIT in diabetic skeletal muscle fibers.

Keywords Diabetic myopathy, High-intensity interval training, Hypertrophy, Kinesin-1, Nuclear movement

Diabetes mellitus (DM) is a metabolic disease characterized by abnormal hyperglycemia due to β-cell failure in insulin production or decreased sensitivity of peripheral tissues such as skeletal muscle, adipose tissue, and liver to insulin[1]. Being the most critical tissue in maintaining glucose homeostasis under insulin-stimulated conditions and major glucose storage and metabolism site, skeletal muscle significantly contributes to diabetic complications. Therefore, a reduction of skeletal muscle mass would compromise blood glucose homeostasis. DM is also associated with skeletal muscle atrophy and loss of myonuclei, which leads to impaired muscle function and metabolism[2]. The diminished skeletal muscle mass in DM is partly related to impairment in skeletal muscle regeneration and recovery from injury[3,4], deficiency in growth and development of skeletal muscle[5], and a shift in the fiber types toward more glycolytic or fast-twitch phenotypes[6,7].

The reduction in skeletal muscle mass in DM also appears to be partly accounted for by altered myonuclei arrangement and morphology[8,9] and loss of myonuclei[10,11]. The normal muscle fibers are characterized with peripherally-located nuclei distribution to maximize the distance between adjacent nuclei[12–14]. Nuclei movement to the center of the myofiber, nucleus movement to the muscle periphery, equidistant spacing of nuclei, and movement of nuclei to the neuromuscular junction (NMJ) are the key steps governing the nuclear positioning process and each step is mediated by different arrays of regulators/motor proteins such as kinesin and dynein motor proteins[12,13]. Such an appropriate nuclear distribution profoundly impacts normal muscle function and development, and several muscle diseases such as CentroNuclear Myopathy (CNM) and dystrophies have been

[1]Department of Exercise Physiology, Faculty of Literature and Human Sciences, Lorestan University, Khoramabad, Iran. [2]Department of Physical Education and Sport Sciences, Faculty of Literature and Humanities, Vali-E-Asr University of Rafsanjan, Rafsanjan, Iran. [3]Department of Exercise Physiology, Faculty of Physical Education and Sport Sciences, Shahid Bahonar University of Kerman, Kerman, Iran. ✉email: rahmati.mas@lu.ac.ir; r_nikooie@uk.ac.ir

linked to mispositioned myonuclei[15]. Although nuclear positioning and its impact on muscle function have been poorly understood in DM, diabetes-induced alteration in morphometric of myonuclei has been reported[8,9]. A decrease in the length and diameters of the myonuclei has been reported in the fore and hind limb muscles of streptozotocin (STZ)-diabetic rats[8]. Skeletal muscle of obese Zucker rats shows a decreased myonuclear numbers per unit fiber length and increased myonuclear domain size, a measure of cytosolic volume per nucleus, compared to healthy animals[11]. A clear cause of such a myonuclear loss in DM is unclear. However, satellite cell dysfunction due to reduced satellite cell proliferation or decreases in myogenic regulatory factor proteins might partly be associated with loss of myonuclei in DM[16,17]. Since myonuclei's properties and number are related to fiber size, it is possible that diabetic-induced muscle atrophy, at least partly, be related to improper myonuclei arrangement and morphology. However, there is no substantial evidence.

Physical exercise is one of the most frequently prescribed tools to manage diabetes complications. High-intensity interval training (HIIT) encompasses short-term, intense intervals (80–120% of maximal oxygen consumption (VO_2max)) alternated with periods of lower intensity for recovery. In addition to having more beneficial metabolic effects than traditional endurance training, HIIT was shown to enhance cross-sectional area (CSA) of soleus, tibialis anterior, and gastrocnemius, and increase skeletal muscle volume and left ventricular mass[18]. Moreover, HIIT augments phosphorylation levels of the mechanistic target of rapamycin (mTOR) signals, p70 S6 kinase (p70S6 K), ribosomal protein S6 (S6)[19] in young and old mice. In addition, HIIT can induce substantial muscle damage, which is a profound stimulus to activate muscle satellite cells[20,21]. Mechanical damage associated with HIIT also causes a progressive increase in myonuclei, increasing muscle fiber size[22,23]. Meanwhile, insulin resistance is more attributable to fast-twitch muscle fiber[24]. Since HIIT is a more effective training stimulus for fast-twitch muscle fibers[24], it could be an efficient training modality improving glucose homeostasis in fast-twitch muscle fibers. These properties make HIIT an appropriate hypertrophic exercise, especially considering the lack of a physiological hypertrophy-inducing protocol for mice.

The primary goal of this study was to test the central hypothesis of whether and how HIIT affects myonuclei arrangement and morphology in skeletal muscle. To evaluate this hypothesis, we investigated: (1) whether HIIT can alleviate diabetes-induced muscle atrophy and myonuclear reduction; (2) the effects of HIIT on myonuclear morphometry impairments and nuclear positioning in diabetic isolated myofibers; (3) possible mechanisms that may be involved in HIIT-induced regulation of myonuclei arrangement and morphology.

Materials and methods

Animals

A total of 60 ten-week-old C57BL/6 male mice were provided and housed four-per-cage in an animal lab under standard conditions (12-hour light/dark cycle in a room at the temperature of 20–25 °C) with access to food and water *ad libitum*. All institutional (as registered under the code: LUNS.REC.1395.170 at Lorestan University of Medical Sciences) and animal research health and ethics guidelines were followed. Moreover, the present study was carried out in compliance with the ARRIVE guidelines. The animals were divided randomly into six groups: (1) healthy control (C, $N=10$), which performed no exercise; control trained (T, $N=10$), which were underwent endurance training; diabetic control (DC, $N=10$), which experienced STZ-induced induction, diabetic trained (DT, $N=10$), which were underwent STZ-induced induction and endurance training; diabetic-RBL (D-RBL, $N=10$), which were underwent STZ-induced induction and subjected to inhibition of kinesin-1 activity and expression in the *gastrocnemius* muscle; and diabetic trained-RBL (DT-RBL, $N=10$), which were underwent STZ-induced induction and endurance training and subjected to inhibition of kinesin-1 activity and expression in the *gastrocnemius* muscle.

Diabetes induction

All the mice were kept in an animal lab for two weeks before the experiments to acclimatize. Subsequently, diabetes was induced through daily intraperitoneal injection with 50 mg/kg body weight of streptozotocin (Sigma, St. Louis, MO, USA) freshly dissolved in 0.1 M citrate buffer (pH 4.5) for five consecutive days[25]. Two weeks later, diabetes was confirmed by measuring tail vein blood glucose level (> 300 mg/ld.) using an Accu Chek Compact Plus blood glucose meter (Roche Diagnostics K.K., Tokyo, Japan). During the study course, blood glucose levels were assessed weekly.

High-intensity interval training (HIIT) protocol

Before starting HIIT protocol, mice were acclimated on the treadmill five times a week at 10 m/min speed for 10 min with no incline. After acclimation protocol for one week, mice were subjected to 3 sessions of HIIT per week for four weeks. Each session consisted of a 5 min warm-up at 10 m/min, eight exercise intervals at the prescribed speed and angle of inclination for 3–5 min, and a 1 min rest interval at 10 m/min between each interval. The inclination angle gradually increased from 5˚ in the first week to 10˚ in the second week and remained at 15˚ in the third and fourth weeks. The treadmill speed was maintained at 15 m/min for all training sessions. No electronic shocks were employed to reduce the stress effect of running on the treadmill during training sessions. Mice were manually assisted back on the treadmill to resume running after landing on the rear part of the treadmill. All HIIT sessions were performed on a leveled motor-driven treadmill (Model T510E, Diagnostic and Research, Taoyuan, Taiwan).

Inhibition of kinesin-1

Daily intraperitoneal injection (30 mg/kg) of Rose Bengal Lactone (RBL; Sigma) was administered to inhibit kinesin-1 activity[26] and suppress its protein levels[27]. Successful inhibition was confirmed via immunoblot in terms of kinesin-1 expression in *gastrocnemius* of the D-RBL compared to the DC group. Western blot analysis

revealed 83% decrease in Kinesin-1 expression in *gastrocnemius* of the D-RBL compared to the DC group (Fig. 1S).

Isolation of mono-myofibers and Immunofluorescence staining

The animals were anesthetized with ketamine (90 mg/kg) and xylazine (10 mg/kg). Following the dissection of the whole muscle from the mice, the gastrocnemius muscle blocks were fixed in 4%PFA in PBS for 2 H at RT. After washes, 40 to 50 mono-myofibers were isolated per staining from each muscle. To detect myonuclei, isolated myofibers were then mounted on glass slides in Vectashield mounting medium containing DAPI (Vector Laboratories, UK). Finally, myofibers were mounted on slides using fluromount Aqueous mounting (Sigma, F4680-25mL) and kept at 4° C. Isolated fibers were analyzed using confocal laser scanning microscopy (Olympus Co. Ltd., Tokyo, Japan).

Fluorescent immunohistochemistry analysis

According to our previous studies, immunofluorescent protocols were carried out[23,28,29]. We used antibodies specific for laminin (L9393, Sigma-Aldrich, St. Louis, MO, USA), Dynein (ab111177, Abcam, Cambridge, MA), KIF5B (ab167429, Abcam, Cambridge, MA), SUN1 (bsm-54420R, Sapphire Bioscience, Australia), Nesprin1 (ab192234, Abcam, Cambridge, MA) and Pax7 (Developmental Studies Hybridoma Bank, Iowa, IA, USA). Secondary antibodies were coupled to FITC, Cy3, or Cy5 (Jackson Immunoresearch Inc). Additionally, antibodies specific to MyHC types I, IIa, and IIb (BA-D5, SC-71, and BF-F3, respectively, University of Iowa Developmental Studies Hybridoma Bank, Iowa City, IA), were supplemented with secondary antibodies coupled to Alexa Fluor 405, 488 and 546 to detect different fiber types (Molecular Probes, Thermo Fisher Scientific, Waltham, MA, USA). Fiber type IIx expression was judged from unstained myofibers.

As previously described, satellite cells were immunolabeled with an antibody directed against Pax7[28]. Only those cells that were Dynein$^+$, KIF5B$^+$, Nesprin1$^+$, SUN1$^{+,}$ and Pax7$^+$ with DAPI$^+$ were counted, expressed as a percentage, and normalized to fiber number. Nuclei exhibiting apoptotic changes were identified with TUNEL-positive apoptotic nuclei using the in situ cell death detection kit, TMRred (Roche Applied Science, Indianapolis, IN, USA), as described previously and expressed per muscle Sect[30]. For confocal analysis, pictures were taken on a TCS SP5 X microscope (Leica Microsystems) at 20X magnification, n and for each condition of each experiment, at least 10–12 fields chosen randomly were analyzedToto measure MHC distribution, CSA, and nuclei per myofiber, images were captured at ×10 and ×20 magnification using a Carl Zeiss AxioImager fluorescent microscope (Carl Zeiss, Jena, Germany). Whole muscle sections were obtained using the mosaic function in Image M1 Software, and muscle fiber cross-sectional area, satellite cells, and myonuclei were analyzed utilizing MyoView[23]. A blinded, well-experienced technician performed all manual counting.

Morphometric analysis of isolated myofibers

In order to measure CSA of isolated myofibers we used the following formulas: $CSA = \pi \times (w/2) \times (t/2)$ where w and t are the width and thickness, respectively. The volume for 100 µm was calculated as CSA × 100 µm (µm^3). Then we measured the following parameters for the myonuclei analysis of isolated myofibers using the analysis particles plugin of Image J software on 2D projections: area (µm^2), maximum diameter length (µm), roundness, and angle (sinus value) of the maximum diameter relative to the long axis of the fibers. Roundness was calculated as 1/(length of the major axis/length of the minor axis). The number of nuclei was counted and illustrated as the number of nuclei/100 µm fiber length or the number of nuclei/volume calculated for 100 µm fiber length. To measure the mean distance between adjacent myonuclei, the three-dimensional coordinates of the geometric center of each nucleus were determined on image stacks using the 3D manager plugin of Image J software.

Western blotting

Approximately 100 mg of gastrocnemius muscle was homogenized in ice-cold RIPA buffer (50 mM Tris- HCl, 1 mM EDTA, 150 mM NaCl, NP40 1%, Na deoxycholate 1%, SDS 1%, protease and phosphatase inhibitor 0.01 M, pH 7.4) and then centrifuged at 14,000 RPM for 15 min at 4 °C. Supernatant was discovered and used to measure protein expression. Protein concentration was determined with Bradford protein assay using BSA as a standard and western blotting was performed as previously described[31]. Molecular weight standards were used to identify appropriate antibody binding. Band densities were determined with ImageJ densitometer software. Primary antibodies used were rabbit anti-Nesprin1 (abcam, cat. # ab192234); anti-KIF5B (cell signaling, cat. # 18148); anti-SUN1 (abcam, cat. # ab103021); anti-Dynein (abcam, cat. # ab23905); and kensin1 (abcam, cat. # ab167429). Goat Anti-Rabbit IgG Antibody, Peroxidase Conjugated (Millipore, cat. # AP132P) was used as the secondary antibody.

Statistical analysis

Statistical analyses were conducted by SPSS software (version 19, SPSS Inc., Chicago, IL, USA). Normality and homogeneity of data were assessed by Shapiro-Wilk and Levene's test, respectively. A within-between (groups × time) repeated measures ANOVA followed by Tukey's post hoc test were used to compare differences in blood glucose and body weight between groups through the study period. Two-way analysis of variance (ANOVA) was performed to determine Dynein, KIF5B, Nesprin1, SUN1, and Pax7 abundances and other variables in experimental groups. The statistical significance level was set at $\alpha = 0.05$. The data were reported as mean ± S.E.M values.

Results

Blood glucose levels, body weight, and *gastrocnemius* mass/body weight

Compared to the C group, the animals from the DC group exhibited significant hyperglycemia and decreased body weight (Table 1), suggesting diabetes was successfully induced in the present study. As Table 1 shows, STZ-induced diabetes significantly increased blood glucose levels ($p < 0.01$), decreased body weight ($p < 0.05$), and attenuated *gastrocnemius* mass/body weight in the DC compared to the C group ($p < 0.05$). Inhibition of kinesin-1 activity exaggerated the effects of diabetes in the D-RBL group. Body weight ($p < 0.05$) and *gastrocnemius* mass/body weight ($p < 0.05$) in the D-RBL were significantly lower compared to the DC group. In animals from the DT group, HIIT significantly decreased blood glucose levels ($p < 0.05$) and increased *gastrocnemius* mass/body weight ($p < 0.05$) compared to the DC group. However, there was still a significant difference between the *C and DT groups*' *gastrocnemius* mass/body weight ($p < 0.05$), suggesting HIIT could not fully restore STZ-induced reduction in *gastrocnemius* mass/body weight. HIIT significantly decreased blood glucose levels in the DT-RBL group compared to the D-BRL ($p < 0.05$). However, neither body weight nor *gastrocnemius* mass/body weight was changed in the animals from the DT-RBL group compared to the D-BRL. Also, *gastrocnemius* mass/body weight ($p < 0.05$) in the DT was significantly higher than in the D-BRL group. These results indicate that HIIT-induced increase in *gastrocnemius* mass/body weight is mediated, at least in part, by changes in nuclear positioning.

HIIT successfully restored STZ-induced muscle atrophy and myonuclear reduction

To understand the effect of diabetes, HIIT, and nuclear positioning on muscle atrophy, muscle fiber CSA, and myonuclear number were studied using laminin and DAPI staining to determine the limit of each myofiber and to detect myonuclei, respectively. As Fig. 1A–C shows, muscle fiber CSA and myonuclear number of single fibers were affected by diabetes. STZ-induced diabetes significantly decreased muscle fiber CSA of *gastrocnemius* muscle in the DC ($p < 0.05$) and the D-BRL ($p < 0.01$) compared to the C group (Fig. 1A, B). The effect of diabetes on muscle fiber CSA of the *gastrocnemius* muscle was more pronounced in the animals from the D-BRL than the DC and there was a significant difference between the two groups ($p < 0.05$). HIIT significantly increased muscle fiber CSA in the *gastrocnemius* muscle of the T and DT groups compared to their counterpart control group (all $p < 0.01$) (Fig. 1B). HIIT restored muscle fiber CSA in the DT to normal value; however, there was still a significant difference between the T and DT regarding the *gastrocnemius* muscle fiber CSA ($p < 0.01$). In animals from the DT-BRL group, HIIT could not restore muscle fiber CSA of *gastrocnemius* to normal value compared to the C group ($p > 0.05$). The difference of muscle fiber CSA of *gastrocnemius* was significant between the DT and D-BRL groups at the end of the study ($p < 0.01$).

Since increasing the number of myonuclei per fiber and maintaining a constant myonuclear domain is vital for muscle hypertrophy[32], we further evaluated the effect of diabetes and HIIT on the magnitude of the myonuclear number. Figure 1C shows that the number of myonuclei per fiber in the DC ($p < 0.01$) and DC-BRL groups ($p < 0.01$) were significantly lower compared to values found in the C group. HIIT significantly increased the number of myonuclei per fiber in the *gastrocnemius* muscle of the T and DT, respectively, compared to their counterpart control group (all $p < 0.01$) (Fig. 1C). HIIT restored the number of myonuclei per fiber in the DT to a normal value; however, there was still a significant difference between the T and DT regarding the number of myonuclei per fiber ($p < 0.01$). In animals from the DT-BRL group, HIIT could not restore the number of myonuclei per fiber to normal value compared to the C group. The difference in the number of myonuclei per fiber was significant between the DT and D-BRL groups at the end of the study ($p < 0.05$).

To determine the mechanism of STZ-induced decrease in myonuclei number and to understand how HIIT rescue it, nuclear apoptotic was compared between the groups. TUNEL-positive nuclei located on the laminin basement membrane was assessed to identify apoptotic nuclei. Compared to the C group, the number of TUNEL-positive nuclei per section of *gastrocnemius* muscle fibers increased significantly in the DC ($p < 0.01$) and to a greater extent in the DC-BRL group ($p < 0.01$) (Fig. 1D, E). While HIIT successfully reduced the number of TUNEL-positive nuclei per section of *gastrocnemius* muscle fibers in the DT compared to the CT group ($p < 0.01$), its effect was almost completely deterred in the DT-BRL group. This data suggests that STZ-induced enhance in nuclear apoptotic declines the number of myonuclei, thereby reducing CSA of *gastrocnemius* muscle. HIIT can alleviate the STZ-induced decline in myonuclei per fiber and muscle CSA by restoring nuclear apoptotic to the normal level. However, proper nuclear positioning is required for HIIT-induced increase in muscle CSA.

groups	Body weight (g)	Blood glucose (mg/dL)	Gas mass/BW (mg/g)
C	30.11 ± 0.61	111 ± 17	4.24 ± 0.47
T	32.64 ± 0.75	105 ± 12	4.41 ± 0.52
DC	26.75 ± 0.57*	539 ± 56**	3.39 ± 0.35*
DT	27.84 ± 0.95*	475 ± 67**†	3.54 ± 0.61*
D-RBL	23.64 ± 0.78*	567 ± 72**	3.15 ± 0.43*
DT-RBL	24.34 ± 0.91*	462 ± 51**†	3.22 ± 0.57*

Table 1. Animals' weight, blood glucose levels, and *gastrocnemius* mass/body weight (gas mass/BW) in the study groups. Values are mean ± S.E.M. Healthy control (C), trained (T), diabetic control (DC), diabetic trained (DT), diabetic-RBL (D-RBL), and diabetic trained-RBL (DT-RBL). *Significant difference with the C ($P < 0.05$), **($P < 0.01$). †Significant difference with the DC ($P < 0.05$). $N = 10$ per group.

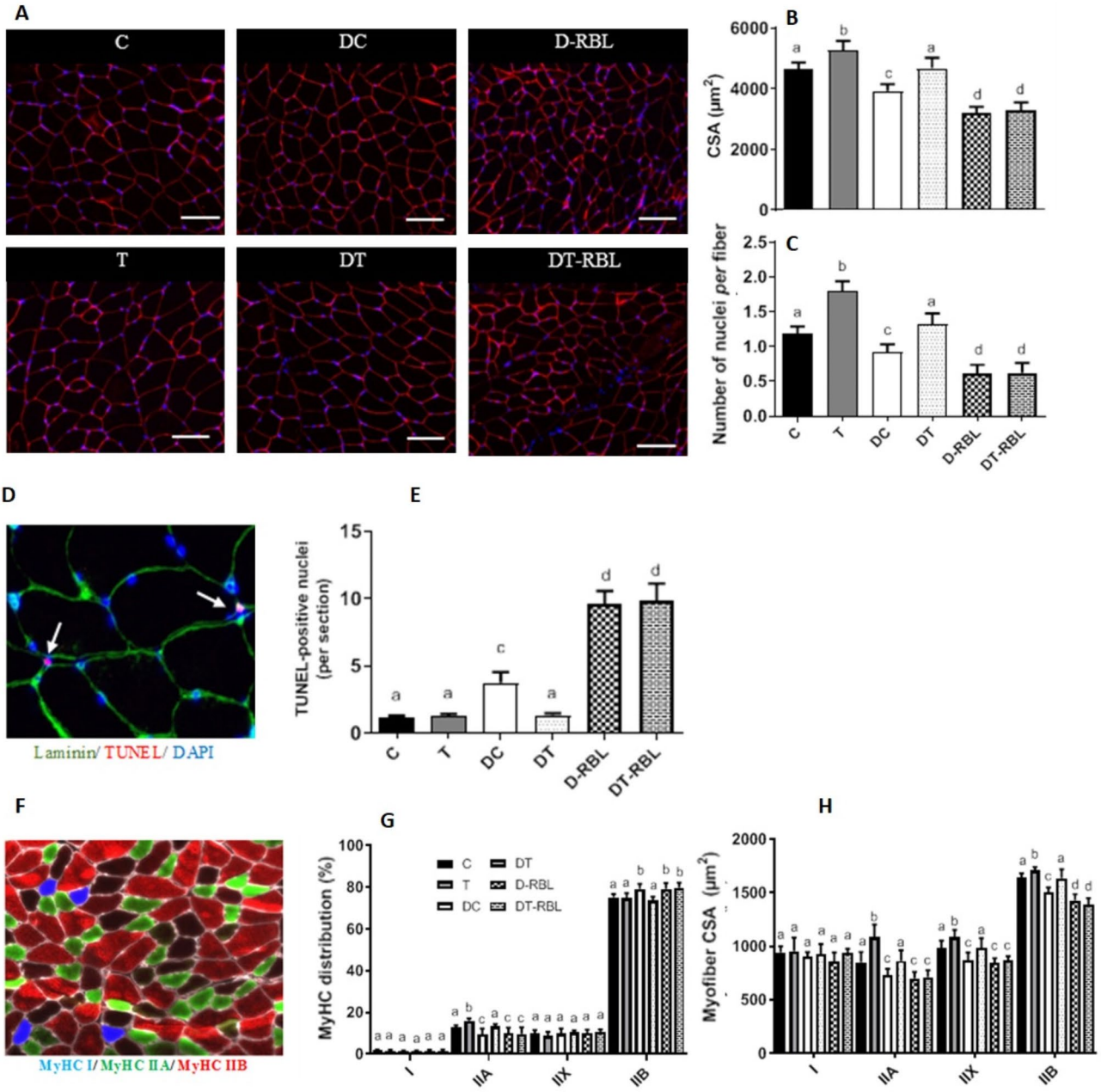

Fig. 1. STZ-induced enhancement in nuclear apoptotic declined the number of myonuclei, thereby reducing muscle CSA. HIIT restored it to the normal level. (**A**) Representative images of muscle CSA analyses: laminin (red) and Hoechst (blue). Scale bars represent 25 μm. (**B**,**C**) Graphs show quantification of *gastrocnemius* muscle CSA (**B**) and number of nuclei per fiber (**C**). (**D**,**E**) Tunnel staining was used to identify TUNEL-positive nuclei located on the laminin basement membrane. (**D**) Representative image showing immunostaining for laminin (green), TUNEL (red), DAPI (blue). Arrows point at TUNEL-positive nuclei located on the laminin basement membrane. (**E**) Graphs show quantification of TUNEL-positive nuclei located on the laminin basement membrane. (**F**) Representative image showing MyHC immunostaining of *gastrocnemius* muscle: MyHC I (blue), MyHC IIA (green), MyHC IIX (black), and MyHC IIB (red). Scale bars represent 25 μm. (**G**,**H**) Graphs show quantification of myofiber CSA in different fiber types (**G**) and MyHC distribution (**H**) of *gastrocnemius* muscle. Values expressed as means ± SD. The different letters indicate a significant difference (ANOVA and subsequent Tukey's HSD, $P < 0.05$).

HIIT abolished STZ-induced muscle fiber-type switching from MyHC IIa to MyHC IIb

Since slow (type I) and fast fibers (types IIa, IIx, and IIb) differentially respond to specific atrophy signals[33], possible changes in the MyHC distribution and CSA in a different types of *gastrocnemius* muscle fibers were evaluated (Fig. 1F–H). The total number of fibers were similar in *gastrocnemius* muscle of the C (6435 ± 964), T (6987 ± 825), DC (6258 ± 798), DT (6514 ± 943), D-RBL (6124 ± 778), DT-RBL (6203 ± 829) and there was

no significant difference among the groups. STZ-induced diabetes significantly decreased MyHC IIa in the *gastrocnemius* muscle of the DC and D-RBL groups. It significantly increased MyHC IIb and IIx in the DC and D-RBL groups compared to the C group (all $p < 0.01$) (Fig. 1G). HIIT restored the number of type IIa and IIb fibers in the DT to normal value; however, there was still a significant difference between the T and DT regarding the number of type IIa and IIb fibers (all $p < 0.01$) (Fig. 1G).

The mean value of MyHC I fiber CSA was identical between all groups (Fig. 1H). However, MyHC IIa, IIx, and IIb fiber CSA were smaller in animals from the DC and D-BRL than in the C group (all $p < 0.05$). Thus the most significant effects of diabetes were a marked decrease in MyHC IIa fibers, an increase in MyHC IIb fibers, and a decline in CSA of MyHC IIa, IIx, and IIb fibers. HIIT significantly increased MyHC IIa, IIx, and IIb fibers CSA in animals from the T and DT compared to their counterpart control groups (all $p < 0.05$, Fig. 1H). However, HIIT did not affect MyHC IIa, IIx, and IIb fibers CSA in the animals from the DT-BRL, and there was no significant difference between the D-BRL and DT-BRL groups at the end of the study. Altogether, these results demonstrated that diabetes causes muscle fiber-type switching from MyHC IIa to MyHC IIb and IIx while exercise training produced a shift toward more significant expression of MyHC IIa. Meanwhile, the results indicate that nuclear positioning is required for HIIT-induced muscle fiber-type switching from MyHC IIb and IIx to MyHC IIa in diabetic animals.

HIIT reserved myonuclear morphometry impairments in diabetic isolated myofibers

A morphometric analysis of myonuclear was performed in *gastrocnemius* isolated muscle fibers further to investigate the effect of diabetes and exercise on myonuclei. We first checked the effect of diabetes and training on the CSA and myonuclei number in *gastrocnemius* isolated muscles fibers (Fig. 2A–C). The results revealed a significant decrease in CSA and myonuclear number in DC and D-BRL groups compared with the C group (all $p < 0.05$) (Fig. 2B). Additionally, inhibition of kinesin-1 activity exaggerated the effects of diabetes in the D-RBL group. CSA ($p < 0.01$) and myonuclear number ($p < 0.01$) of *gastrocnemius* isolated myofibers in the DT-BRL group were significantly lower than the DC group (Fig. 2B, C). In the T and DT groups, HIIT significantly increased CSA and the number of myonuclei compared to their counterpart control group (all $p < 0.05$, Fig. 2B, C). Nevertheless, inhibition of kinesin-1 activity abolished the positive effect of HIIT on, CSA and the number of myonuclei in gastrocnemius isolated muscles fibers of the animals from the DT-BRL.

We were next interested to know whether and how diabetes and exercise can affect myonuclear morphometric properties. The results are reported in (Fig. 2D–G). STZ-induced diabetes significantly decreased the nuclei volume and maximum diameter in DC and D-BRL groups compared to the C group (all $p < 0.05$; Fig. 2D, E). The effect of diabetes was more pronounced in the animals from the D-BRL group. Their maximum diameter and volume of the nuclei were significantly lower than those values found in the DC group (all $p < 0.05$). The area of the myonuclei was similar between the C and DC groups but had a lower value in the D-BRL group than the DC ($p < 0.05$; Fig. 2F). In T and DT trained groups, HIIT significantly increased volume of the nuclei (all $p < 0.01$; Fig. 2D) and the maximum diameter (all $p < 0.01$; Fig. 2E) compared to their counterpart control group. The beneficial effects of HIIT on the maximum diameter and volume of the nuclei were deterred by inhibition of kinesin-1 activity and there was no significant difference between the DC-BRL and TD-BRL at the end of the study. Moreover, the mean values of nuclei roundness were identical between all groups (all $p > 0.05$, Fig. 2G). These results revealed a protective effect of HIIT from a slight modification of the nuclear properties in *gastrocnemius* isolated myofibers of diabetic animals. The results also indicate that normal nuclear positioning is required for the changes in myonuclear morphometric properties associated with HIIT in diabetic animals.

HIIT improves nuclear positioning in diabetic isolated myofibers

Since normal nuclear positioning is required for different muscle functions, including muscle mass[34], we next further question whether there is a change in the myonuclear positioning of the *gastrocnemius* isolated muscles fibers. The sinus of the maximum diameter angles relative to the fiber's long axis and the distance between adjacent myonuclei were calculated and compared among the groups. Compared with the C group, a decrease in sinus value was found in isolated fibers of DC ($P < 0.05$, Fig. 2H) and DC-BRL groups ($p < 0.001$, Fig. 2H). Sinus values were significantly lower in the DC-BRL group ($p < 0.05$, Fig. 2H) compared with the DC group. Sinus values were similar between the C and T groups and between the DC-BRL and DT-BRL groups. However, HIIT restored diminished sinus values in the DT to normal value and sinus values were significantly higher in the DT than the DC group (all $p < 0.05$, Fig. 2H). Altogether, these data argue for a slight but significant modification of the spatial organization of myonuclei in the atrophied myofibers from STZ-induced diabetic mice.

To calculate the distance between adjacent myonuclei, the spatial organization of nuclei was first determined in *gastrocnemius* isolated myofibers by measuring the nearest neighbor distance, i.e., the distance from each nucleus to the nearest nucleus measured using the three-dimensional coordinates of their geometric center. Compared with the C group, diabetes caused an increase of the mean distance between adjacent myonuclei in DC ($P < 0.05$, Fig. 2I) and DC-BRL groups ($p < 0.001$, Fig. 2I). Compared with the DC group, the mean distance between adjacent myonuclei was significantly higher in the DC-BRL group ($p < 0.05$, Fig. 2I). In the T and DT groups, HIIT significantly decreased the mean distance between adjacent myonuclei (all $p < 0.01$; Fig. 2I) compared to their counterpart control group. HIIT did not affect the mean distance between adjacent myonuclei in the DT-BRL and there was no significant difference between the DC-BRL and DT-BRL. These results suggest that diabetes by reducing the distance between adjacent myonuclei could lead to the abnormal spatial organization of nuclei in myofibers, while HIIT can restore the normal distance between adjacent myonuclei.

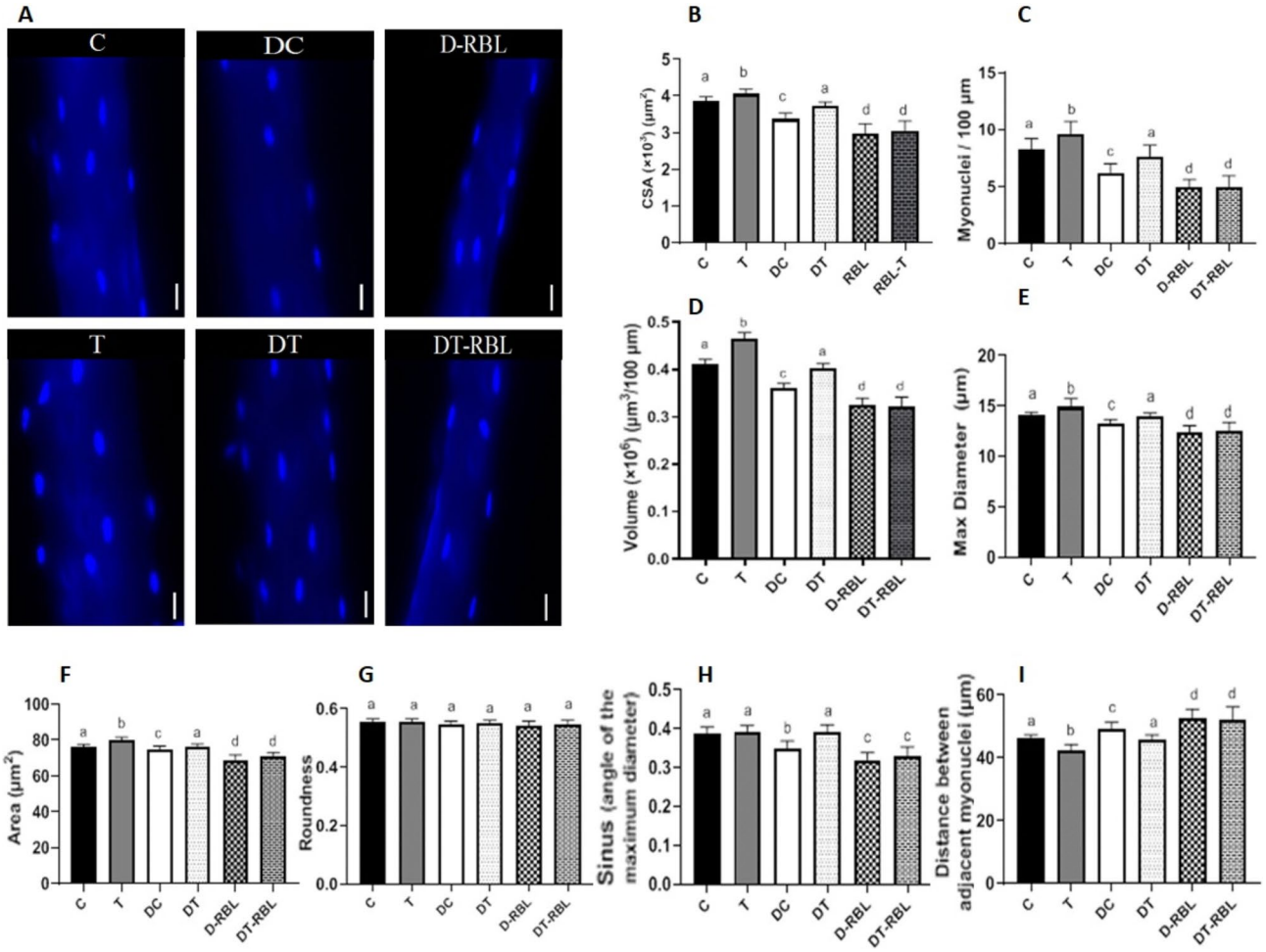

Fig. 2. Induction of diabetes was associated with disturbance in morphometric characteristics of myonuclei and nuclear positioning in *gastrocnemius* isolated myofibers, and HIIT rescued it to the normal level. (**A**) Confocal microscopy images of single muscle fibers of *gastrocnemius* muscle stained by DAPI. The illustrated image corresponds to the XY projection of one image stack. Scale bars represent 25 μm. (**B**,**C**) Graphs show quantification of CSA ($\times 10^3$) (μm^2) (B) and myonuclei number (**C**) in *gastrocnemius* isolated muscle fibers. (**D**–**G**) Graphs show morphometric characteristics of myonuclei: quantification of the nuclear volume ($\times 10^6$) (μm^2/100 µm) (**D**), the maximum diameter of the nuclei (µm) (**E**), nuclear area (μm^2) (**F**), nuclear roundness (**G**) in *gastrocnemius* isolated muscles fibers. (**H**,**I**) graphs show nuclear positioning indexes in *gastrocnemius* isolated myofibers: sinus of the angle of the maximum diameter of nuclei relative to the axis of the fiber (**H**) and nearest neighbor distance of myonuclei of isolated fibers (**I**). Values expressed as means ± SD. The different letters indicate a significant difference (ANOVA and subsequent Tukey's HSD, $P < 0.05$).

HIIT attenuated diabetes-induced abnormality in the nuclear linker and motor proteins involved in nuclear positioning

To determine how diabetes and HIIT affect nuclear positioning in skeletal muscle, we next measured the expression of motor proteins involved in nuclear positioning (KIF5B and dynein) and proteins involved in linking the nucleus to the cytoskeleton (Nesprin1 and SUN1). KIF5B, dynein, and Nesprin1 numbers were significantly lower in the DC group than those values found in the C group (all $p < 0.01$; Figs. 3A–F and 4A–C). In contrast, the expression of SUN1 was not affected by STZ-induced diabetes (Fig. 4D–F). Inhibition of kinesin-1 activity did not affect the expression of protein analyzed. HIIT significantly increased the expression of KIF5B, dynein, and Nesprin1in T and DT groups compared to their counterpart control groups (all $p < 0.01$). The expression of SUN1 was not affected by HIIT, neither in T nor in DT groups. The effects of HIIT on KIF5B, dynein and Nesprin1 expression were deterred by inhibition of kinesin-1 activity and there was no significant difference for any protein analyzed between the DC-BRL and DT-BRL.

To further confirm of diabetes and HIIT effect on nuclear positioning, we also measured the expression of KIF5B, dynein, Nesprin1, and SUN1 in skeletal muscle by western blotting. STZ-induced diabetes decreased the expression of KIF5B (DC, 43%, $p < 0.05$; DC-BRL, 58%, $p < 0.01$, Fig. 3E, F), dynein (DC, 40%, $p < 0.05$; DC-BRL, 48%, $p < 0.01$, Fig. 3E, F), and Nesprin1 (DC, 21%, $p < 0.05$; DC-BRL, 30%, $p < 0.05$, Fig. 4C, F) compared to the C group and had no effect on SUN1 expression. HIIT increased the expression of KIF5B (T, 74%, $p < 0.01$; DT, 255%, $p < 0.01$, Fig. 3E, F), dynein (T, 55%, $p < 0.05$; DT, 78%, $p < 0.05$, Fig. 4C, F), and Nesprin1 (T, 59%, $p < 0.05$;

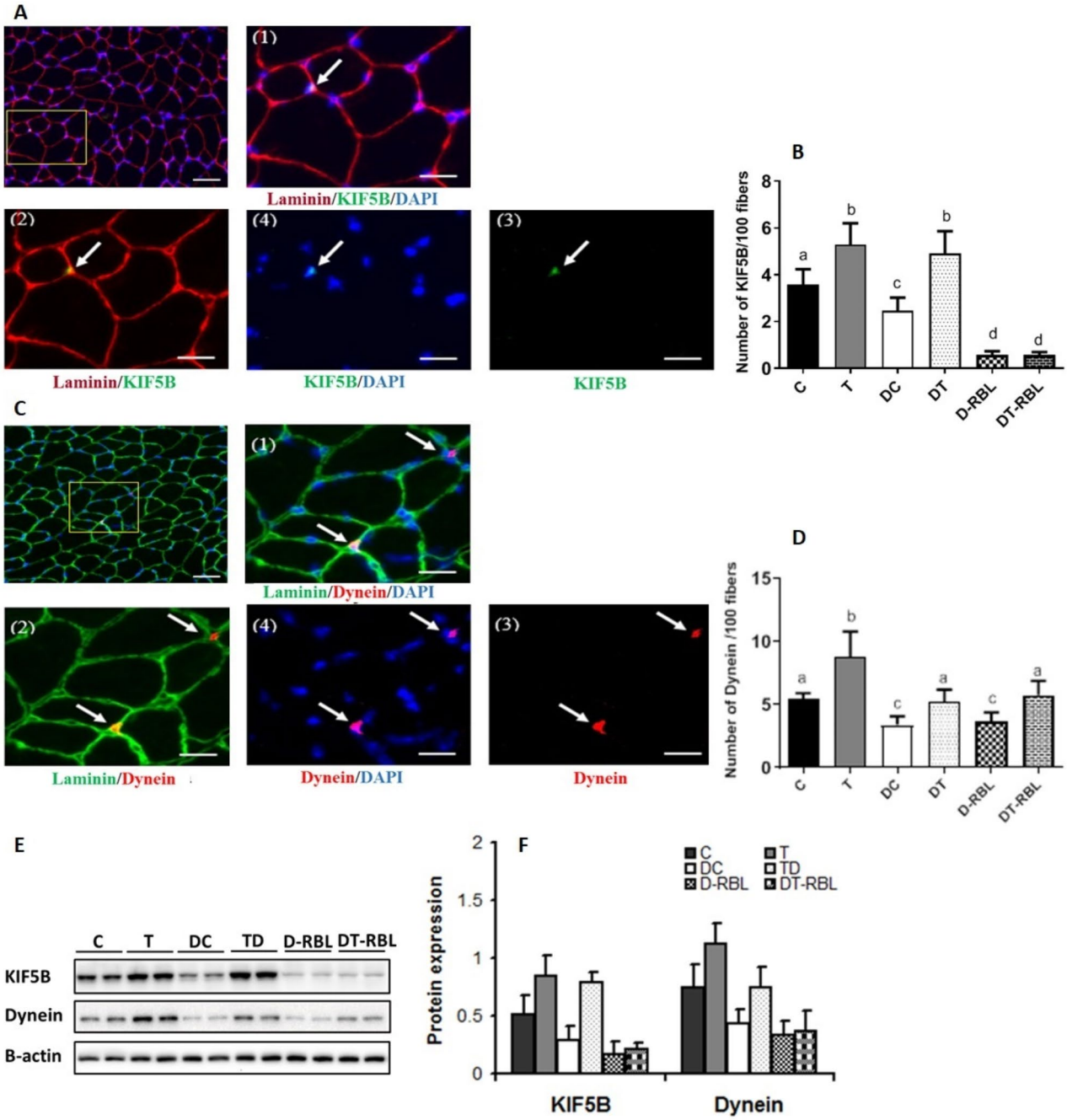

Fig. 3. STZ-induced diabetes disturbance in nuclear positioning was mediated by reduced expression of motor proteins involved in nuclear positioning. (**A**) Representative image of Kif5B analysis. (**A** 1–4) Higher magnification of selected area (yellow box) in image (**A**) showing Laminin (red), Kif5B (green), and myonuclei (blue). (**B**) Quantification of number of Kif5B^{+}/100 fibers. (**C**) Representative image of Dynein analysis. (C1-4) Higher magnification of selected area (yellow box) in image (**D**) showing Laminin (green), Dynein (red), and myonuclei (blue). (**D**) Quantification of number of Dynein^{+}/100 fibers. Scale bars represent 50 μm. (**E**,**F**) In-gel profile and bar plots for densitometric scanning analysis of KIF5B and Dynein. The fold changes in expression levels of the proteins analyzed were normalized for B-actin. Values expressed as means ± SD. The different letters indicate a significant difference (ANOVA and subsequent Tukey's HSD, $P < 0.05$).

DT, 57%, $p < 0.05$, Fig. 4C, F) compared to their counterpart groups, and had no effect on SUN1 expression. The effects of HIIT on KIF5B, dynein and Nesprin1 expression were deterred by inhibition of kinesin-1 activity and there was no significant difference for any protein analyzed between the DC-BRL and DT-BRL. Altogether, these results suggest that muscle nuclear positioning machinery is negatively affected by STZ-induced diabetes and HIIT can restore their expression to normal levels.

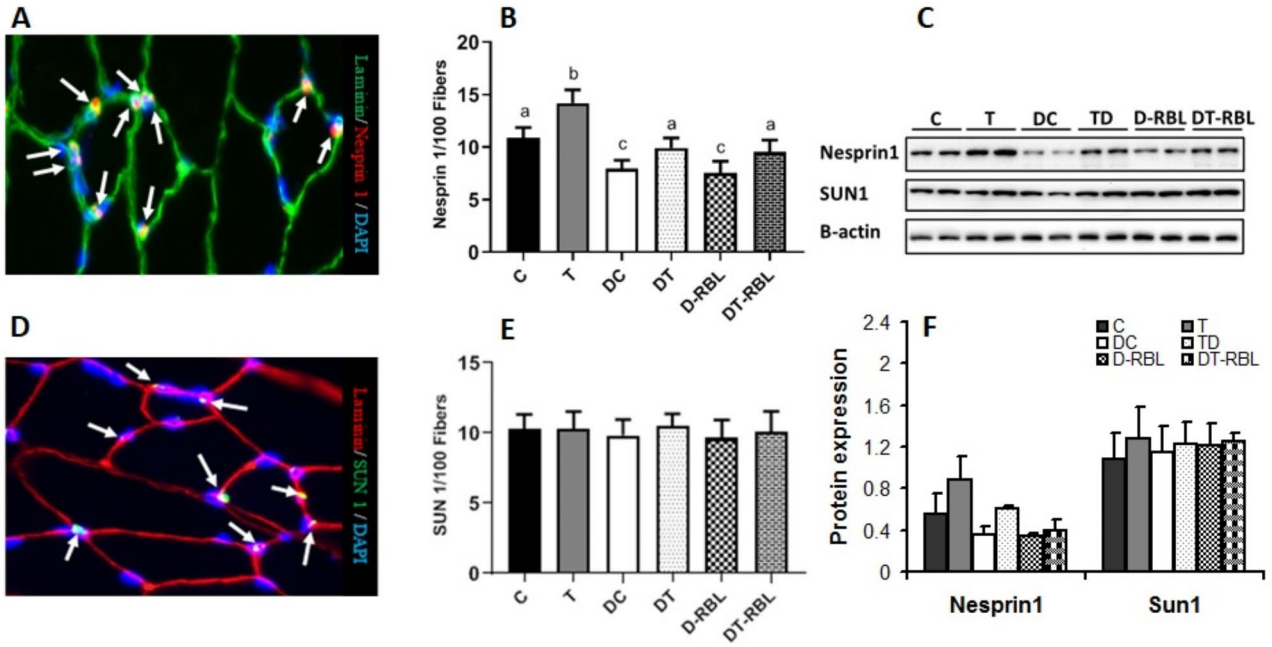

Fig. 4. Suppressed expression of Nesprin1, but not SUN1, was involved in STZ-induced diabetes disturbance in nuclear positioning, and HIIT rescued it to the normal level. (**A**) Representative image of Nesprin1 analysis: Laminin (green), Nesprin1 (red), and myonuclei (blue). (**B**) Quantification of number of Nesprin1/100 fibers. Scale bars represent 50 μm. (**C**,**F**) In-gel profile and bar plots for densitometric scanning analysis of Nesprin1. The fold changes in expression levels of the proteins analyzed were normalized for B-actin. (**D**) Representative image of SUN1 analysis: Laminin (red), SUN1 (green), and myonuclei (blue). (**E**) Quantification of number of Kif5B^{+}/100 fibers. Scale bars represent 50 μm. (**C**,**F**) In-gel profile and bar plots for densitometric scanning analysis of SUN1. The fold changes in expression levels of the proteins analyzed were normalized for B-actin. Values expressed as means ± SD. The different letters indicate a significant difference (ANOVA and subsequent Tukey's HSD, $P < 0.05$).

HIIT effectively restored lower satellite cell content in diabetic myofibers

Given that myonuclei are post-mitotic, myonuclear accretion is thought to occur through the fusion of satellite cells to the growing myofiber, thereby contributing to a nucleus[14]. Therefore, we next decided to quantify the number of satellite cells to determine the cause of lower myonuclear number in *gastrocnemius* muscle of diabetic mice. We evaluated the number of Pax7^{+} cells in 100 fibers (Fig. 5). The number of Pax7^{+} cells significantly decreased in the *gastrocnemius* muscle of the DC ($P < 0.05$, Fig. 5A, B) and DC-BRL groups ($p < 0.001$, Fig. 5A, B) compared to the C group. The effect of diabetes was more pronounced in the animals from the DC-BRL than in the DC. The number of Pax7^{+} cells was significantly lower in this group ($p < 0.05$, Fig. 5). In the T and DT groups, HIIT significantly increased the number of Pax7^{+} cells ($p < 0.01$; $p < 0.01$) compared to their counterpart control group. HIIT did not affect the number of Pax7^{+} cells in the DT-BRL, and there was no significant difference between the DC-BRL and DT-BRL groups. Altogether, our results suggest that *gastrocnemius* muscle atrophy in diabetic mice is related to a lower nuclear number which might be caused by failed nuclear accretion from satellite cells. While HIIT is capable of producing significant muscle hypertrophic stimuli by restoring satellite cell numbers.

Discussion

The current study examined whether and how diabetes and HIIT affected myonuclear positioning and examined how HIIT-induced possible changes in myonuclear positioning contribute to STZ-induced muscle atrophy. Three novel results were ascertained and discussed in more detail as follows: (1) STZ-induced diabetes causes myonuclear reduction, impairs myonuclear morphometry, and disrupts nuclear positioning in diabetic isolated myofibers, thereby causing muscle atrophy; (2) HIIT successfully restores STZ-induced impairment in myonuclear morphometry and nuclear positioning, thereby causing muscle hypertrophy; (3) HIIT-induced muscle hypertrophy is mediated by improvement in nuclear positioning in STZ-induced diabetic myofibers.

Consistent with previous studies[35–37], our results showed that STZ-induced diabetes causes muscle atrophy associated with a myonuclear reduction in diabetic mice. Although the exact mechanism of STZ-induced muscle atrophy is unclear, enhanced activity of WWP1/KLF15 axis, increased p65 content[36], FoxO transcription factors (FoxOs)-induced increases in proteolytic pathways[37] are some of the mechanisms involved in STZ-induced muscle atrophy. In this context, we were interested in knowing whether STZ-induced muscle atrophy is related to myonuclear morphometric properties and nuclear positioning. We observed that gastrocnemius mass/body weight, muscle fiber CSA of the *gastrocnemius*, and myonuclear number were lower in the diabetic animals than

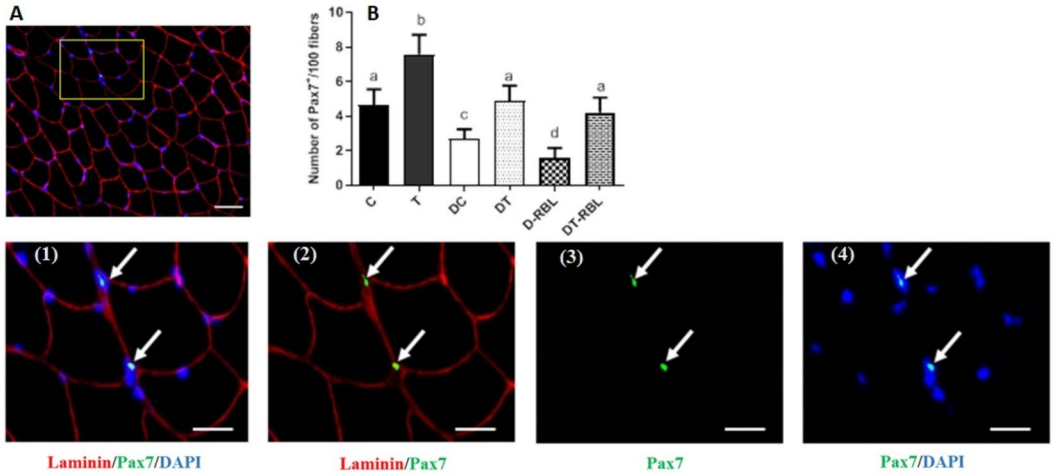

Fig. 5. STZ-induced atrophy in *gastrocnemius* muscle was related to a failed nuclear accretion from satellite cells. HIIT was capable of restoring satellite cell numbers. (**A**) Representative image of Pax7 analysis. (**A** 1–4) Higher magnification of selected area (yellow box) in image (**A**) showing Laminin (red), Pax7 (green), and myonuclei (blue). Scale bars represent 50 µm. (**B**) Quantification of the number of $Pax7^+$/100 fibers. Values expressed as means ± SD. The different letters indicate a significant difference (ANOVA and subsequent Tukey's HSD, $P < 0.05$).

in healthy mice. All these changes were associated with disrupted nuclear positioning, quantified by the distance between adjacent myonuclei, sinus values (the angle of the maximum diameter), and improper myonuclear morphometric properties, quantified by the maximum diameter and volume of the nuclei, in the STZ-induced diabetic mice. To investigate the cause-and-effect relationship between STZ-induced muscle atrophy and nuclear positioning, kinesin-1 activity was inhibited by, i.p., injection of Rose Bengal Lactone in diabetic animals. Their responses were compared with those of the diabetic control animals. We selected Kinesin-1 because the interaction between KIF5b/Kinesin-1 and a Microtubule Associated Protein (Map7) builds a complex required for achieving and maintaining proper nuclear positioning[38]. Thus drug inhibition of Kinesin-1 activity is a usual method to disrupt myonuclear positioning[27], especially considering that conditional muscle knock-out for Kinesin-1 leads to animal death due to severe dystrophy of skeletal muscles[39]. The present study results indicate that inhibition of kinesin-1 successfully disrupted nuclear positioning in diabetic animals and exaggerated STZ-induced muscle atrophy compared with those of the diabetic control animals, suggesting STZ-induced muscle atrophy is mediated, at least in part, by changes in nuclear positioning.

Skeletal muscle characteristics, including fiber type distribution and glycolytic capacity, may be linked to alterations in insulin action; a high percentage of more glycolytic fibers would be directly related to insulin sensitivity[7]. Consistent with previous studies in diabetic patients[40,41] our results show that STZ-induced diabetes causes a higher percentage of type IIB fibers in *gastrocnemius* muscle of diabetic mice. Although, our result showed that HIIT was effective enough to restore skeletal muscle fiber type distribution in STZ-induced diabetic mice.

To understand how STZ-induced diabetes disrupts nuclear positioning, muscle satellite cell content and the expression of motor proteins involved in nuclear positioning were evaluated. Our results showed that STZ-induced diabetes decreases the number of $Pax7^+$ cells in skeletal muscle of diabetic mice, suggesting STZ-induced diabetes suppresses muscle stem cell proliferation in skeletal muscle. Since myonuclei are post-mitotic, satellite cell-mediated myonuclear accretion is required for skeletal muscle fiber hypertrophy[14]. In this regard, our results indicate that HIIT successfully restores satellite cell contents in STZ-induced diabetic myofibers. These findings suggest that skeletal muscle fiber atrophy in STZ-induced diabetic mice is related to the lower nuclear number, which might also be caused by failed nuclear accretion from satellite cells, while HIIT, thereby restoring satellite cell numbers, can produce significant physiological changes in hypertrophic stimuli. We also found that diabetes decreases the number of skeletal muscle motor proteins involved in nuclear positioning, including KIF5B and dynein. Moreover, myonuclei rigidity is dependent on proteins of the LINC complex such as Nesprin1 and SUN1[42]. In the present study, we found that diabetes triggers Nesprin1, which may explain the improper positioning of the muscle nuclei in STZ-induced diabetic animals. These data suggest a complex interplay between factors that maintain peripheral myonuclei localization and demonstrate that reduction in motor proteins and Nesprin1 contribute to improper myonuclei positioning in diabetes, while HIIT can restore these abnormalities.

Various diseases can directly affect myonuclear positioning. In a heterogeneous group of inherited muscle diseases, CentroNuclear Myopathies (CNMs) are characterized pathologically by an abnormal localization of myonuclei in the center of myofibers[15]. Different genes implicated in various CNMs such as Mtm1, Amphyphisin-2/BIN1, Dynamin-2, and Hacd1 have already been identified[43,44]. In addition, in the case of sarcopenic skeletal muscle, myonuclear positioning is changed and peripheral myonuclei are also progressively lost[45].

Despite the significant findings, the current study has several limitations. As a proof-of-concept study investigating the effects of high-intensity interval training (HIIT) on diabetes-induced myofiber atrophy, experiments were conducted exclusively on male diabetic mice. Further studies are needed to assess whether similar changes occur in female diabetic mice, as sex may influence the regulation of muscle fibers and myonuclear arrangement[46]. This is particularly relevant given that gender differences could impact the generalizability of the findings. Although this study provides important insights into the effects of high-intensity interval training (HIIT) on diabetes-induced myofiber atrophy using an in vivo model, it is important to acknowledge that the current study lacks in vitro investigations. In vitro models would allow for a more detailed exploration of the underlying molecular and cellular mechanisms involved in the observed effects. Specifically, these models could help identify the precise signaling pathways that regulate myonuclear accretion, hypertrophy, and muscle fiber morphology in diabetic conditions. Future research should aim to integrate both in vivo and in vitro approaches to further elucidate the mechanisms through which HIIT influences muscle regeneration and remodeling at the cellular level. By utilizing in vitro systems, we can more accurately assess the role of key regulatory factors, such as muscle stem cells, myonuclear dynamics, and metabolic signaling, providing a comprehensive understanding of the therapeutic potential of HIIT for individuals with diabetes.

Altogether, STZ-induced diabetes changes myonuclear positioning and morphology, while HIIT successfully restores these impairments. Thus, HIIT might serve as an adjunct therapy in diabetes. However, further work is necessary to fully understand the underlying mechanisms.

Data availability

The data that support the findings of this study are available from the corresponding author (Dr Masoud Rahmati; rahmati.mas@lu.ac.ir) upon reasonable request.

Received: 24 August 2024; Accepted: 19 February 2025
Published online: 26 February 2025

References

1. Tan, S. Y. et al. Type 1 and 2 diabetes mellitus: A review on current treatment approach and gene therapy as potential intervention. *Diabetes Metab. Syndrome Clin. Res. Rev.* **13** (1), 364– 72 (2019).
2. Katta, A. et al. Impaired overload-induced hypertrophy is associated with diminished mTOR signaling in insulin-resistant skeletal muscle of the obese Zucker rat. *Am. J. Physiol. Regul. Integr. Comp. Physiol.* **299** (6), R1666–R75 (2010).
3. Krause, M. P. et al. Impaired macrophage and satellite cell infiltration occurs in a muscle-specific fashion following injury in diabetic skeletal muscle. *PloS One* **8** (8), e70971 (2013).
4. Vignaud, A. et al. Diabetes provides an unfavorable environment for muscle mass and function after muscle injury in mice. *Pathobiology* **74** (5), 291–300 (2007).
5. D'Souza, D. M., Al-Sajee, D. & Hawke, T. J. Diabetic myopathy: impact of diabetes mellitus on skeletal muscle progenitor cells. *Front. Physiol.* **4**, 379 (2013).
6. Kim, J. et al. The preventive effects of 8 weeks of resistance training on glucose tolerance and muscle fiber type composition in Zucker rats. *Diabetes Metab. J.* **39** (5), 424–433 (2015).
7. Yasuda, K. et al. Growth-related changes in skeletal muscle fiber type and insulin resistance in diabetic Otsuka Long-Evans Tokushima fatty rats. *Acta Histochem. Cytochem.* **34** (5), 371–382 (2001).
8. Aughsteen, A. A., Khair, A. & Suleiman, A. A. Quantitative morphometric study of the skeletal muscles of normal and streptozotocin-diabetic rats. *Jop* **7** (4), 382–389 (2006).
9. Ozaki, K., Matsuura, T. & Narama, I. Histochemical and morphometrical analysis of skeletal muscle in spontaneous diabetic WBN/Kob rat. *Acta Neuropathol.* **102** (3), 264–270 (2001).
10. Ato, S., Kido, K., Sato, K. & Fujita, S. Type 2 diabetes causes skeletal muscle atrophy but does not impair resistance training-mediated myonuclear accretion and muscle mass gain in rats. *Exp. Physiol.* **104** (10), 1518–1531 (2019).
11. Peterson, J. M., Bryner, R. W. & Alway, S. E. Satellite cell proliferation is reduced in muscles of obese Zucker rats but restored with loading. *Am. J. Physiol. Cell Physiol.* **295** (2), C521–C8 (2008).
12. Folker, E. & Baylies, M. Nuclear positioning in muscle development and disease. *Front. Physiol.* **4**, 363 (2013).
13. Roman, W. & Gomes, E. R. (eds) *Nuclear Positioning in Skeletal Muscle. Seminars in Cell & Developmental Biology* (Elsevier, 2018).
14. Rahmati, M., McCarthy, J. J. & Malakoutinia, F. Myonuclear permanence in skeletal muscle memory: a systematic review and meta-analysis of human and animal studies. *J. Cachexia Sarcopenia Muscle* **13** (5), 2276–2297 (2022).
15. Jungbluth, H. & Gautel, M. Pathogenic mechanisms in centronuclear myopathies. *Front. Aging Neurosci.* **6**, 339 (2014).
16. Aragno, M. et al. Oxidative stress impairs skeletal muscle repair in diabetic rats. *Diabetes* **53** (4), 1082–1088 (2004).
17. Kim, Y-B., Peroni, O. D., Franke, T. F. & Kahn, B. B. Divergent regulation of Akt1 and Akt2 isoforms in insulin target tissues of obese Zucker rats. *Diabetes* **49** (5), 847–856 (2000).
18. Kemi, O. J., Loennechen, J. P., Wisløff, U. & Ellingsen, Ø. Intensity-controlled treadmill running in mice: cardiac and skeletal muscle hypertrophy. *J. Appl. Physiol.* **93** (4), 1301–1309 (2002).
19. Fyfe, J. J., Bishop, D. J., Zacharewicz, E., Russell, A. P. & Stepto, N. K. Concurrent exercise incorporating high-intensity interval or continuous training modulates mTORC1 signaling and MicroRNA expression in human skeletal muscle. *Am. J. Physiol. Regul. Integr. Comp. Physiol.* **310** (11), R1297–R311 (2016).
20. Damas, F. et al. Resistance training-induced changes in integrated myofibrillar protein synthesis are related to hypertrophy only after attenuation of muscle damage. *J. Physiol.* **594** (18), 5209–5222 (2016).
21. Pugh, J. K., Faulkner, S. H., Turner, M. C. & Nimmo, M. A. Satellite cell response to concurrent resistance exercise and high-intensity interval training in sedentary, overweight/obese, middle-aged individuals. *Eur. J. Appl. Physiol.* **118** (2), 225–238 (2018).
22. Goh, Q. et al. Myonuclear accretion is a determinant of exercise-induced remodeling in skeletal muscle. *Elife* **8**, e44876 (2019).
23. Rahmati, M. & Rashno, A. Automated image segmentation method to analyse skeletal muscle cross section in exercise-induced regenerating myofibers. *Sci. Rep.* **11** (1), 1–16 (2021).
24. Koh, H-C-E. et al. High-intensity interval, but not endurance, training induces muscle fiber type-specific subsarcolemmal lipid droplet size reduction in type 2 diabetic patients. *Am. J. Physiol. Endocrinol. Metab.* **315** (5), E872–E84 (2018).
25. Sun, N., Yang, G., Zhao, H., Savelkoul, H. F. & An, L. Multidose streptozotocin induction of diabetes in BALB/c mice induces a dominant oxidative macrophage and a conversion of TH1 to TH2 phenotypes during disease progression. *Mediat. Inflamm.* **2005** (4), 202–209 (2005).
26. Hopkins, S. C., Vale, R. D. & Kuntz, I. D. Inhibitors of Kinesin activity from structure-based computer screening. *Biochemistry* **39** (10), 2805–2814 (2000).

27. Lin, J-W. et al. Dexamethasone accelerates muscle regeneration by modulating kinesin-1-mediated focal adhesion signals. *Cell. Death Discov.* **7** (1), 1–16 (2021).
28. Rahmati, M. & Taherabadi, S. J. The effects of exercise training on Kinesin and GAP-43 expression in skeletal muscle fibers of STZ-induced diabetic rats. *Sci. Rep.* **11** (1), 1–9 (2021).
29. Bostani, M., Rahmati, M. & Mard, S. A. The effect of endurance training on levels of LINC complex proteins in skeletal muscle fibers of STZ-induced diabetic rats. *Sci. Rep.* **10** (1), 1–10 (2020).
30. Yoshihara, T. et al. Dietary Astaxanthin supplementation attenuates disuse-induced muscle atrophy and myonuclear apoptosis in the rat soleus muscle. *J. Physiol. Sci.* **67**, 181–190 (2017).
31. Nikooie, R., Jafari-Sardoie, S., Sheibani, V. & Nejadvaziri Chatroudi, A. Resistance training-induced muscle hypertrophy is mediated by TGF-β1-Smad signaling pathway in male Wistar rats. *J. Cell. Physiol.* **235** (7–8), 5649–5665 (2020).
32. BruusgaardJC, JohansenI, EgnerI, RanaZ & GundersenK Myonuclei acquired by overload exercise precede hypertrophy and are not lost on detraining. *Proc. Natl. Acad. Sci.* **107** (34), 15111–15116 (2010).
33. Wang, Y. & Pessin, J. E. Mechanisms for fiber-type specificity of skeletal muscle atrophy. *Curr. Opin. Clin. Nutr. Metab. Care* **16** (3), 243 (2013).
34. Metzger, T. et al. MAP and kinesin-dependent nuclear positioning is required for skeletal muscle function. *Nature* **484** (7392), 120–124 (2012).
35. Hirata, Y. et al. Hyperglycemia induces skeletal muscle atrophy via a WWP1/KLF15 axis. *JCI Insight* **4**(4). (2019).
36. Kelleher, A. R., Fairchild, T. J. & Keslacy, S. STZ-induced skeletal muscle atrophy is associated with increased p65 content and downregulation of insulin pathway without NF-κB canonical cascade activation. *Acta Diabetol.* **47** (4), 315–323 (2010).
37. O'Neill, B. T. et al. FoxO transcription factors are critical regulators of diabetes-related muscle atrophy. *Diabetes* **68** (3), 556–570 (2019).
38. Wilson, M. H. & Holzbaur, E. L. Nesprins anchor kinesin-1 motors to the nucleus to drive nuclear distribution in muscle cells. *Development* **142** (1), 218–228 (2015).
39. Wang, Z. et al. Kif5b controls the localization of myofibril components for their assembly and linkage to the myotendinous junctions. *Development* **140** (3), 617–626 (2013).
40. Hickey, M. S. et al. Skeletal muscle fiber composition is related to adiposity and in vitro glucose transport rate in humans. *Am. J. Physiol. Endocrinol. Metab.* **268** (3), E453–E7 (1995).
41. MÅrin, P., Andersson, B., Krotkiewski, M. & Björntorp, P. Muscle fiber composition and capillary density in women and men with NIDDM. *Diabetes Care* **17** (5), 382–386 (1994).
42. Razafsky, D. & Hodzic, D. Nuclear envelope: positioning nuclei and organizing synapses. *Curr. Opin. Cell Biol.* **34**, 84–93 (2015).
43. Bitoun, M. et al. Mutations in dynamin 2 cause dominant centronuclear myopathy. *Nat. Genet.* **37** (11), 1207–1209 (2005).
44. Muhammad, E. et al. Congenital myopathy is caused by mutation of HACD1. *Hum. Mol. Genet.* **22** (25), 5229–5236 (2013).
45. Edström, E. et al. Factors contributing to neuromuscular impairment and sarcopenia during aging. *Physiol. Behav.* **92** (1–2), 129–135 (2007).
46. Deasy, B. M. et al. A role for cell sex in stem cell–mediated skeletal muscle regeneration: female cells have higher muscle regeneration efficiency. *J. Cell Biol.* **177** (1), 73–86 (2007).

Author contributions

M.R. Supervision, Project administration, Methodology, Investigation, Software, Validation, Resources, Visualization, Conceptualization, Writing—original draft, Data curation. R.N. Methodology, Investigation, Software, Validation, Resources, Visualization, Conceptualization, Data curation, Writing—review & editing. Masoud Rahmati and Rohollah Nikooie should be considered the joint corresponding author.

Funding

This work was supported by the Lorestan university Grant (95101418). We gratefully acknowledge the support of all our collaborators.

Declarations

Competing interests

The authors declare no competing interests.

Additional information

Supplementary Information The online version contains supplementary material available at https://doi.org/10.1038/s41598-025-91259-7.

Correspondence and requests for materials should be addressed to M.R. or R.N.

Reprints and permissions information is available at www.nature.com/reprints.

Publisher's note Springer Nature remains neutral with regard to jurisdictional claims in published maps and institutional affiliations.